# Measurements of local droplet velocities in horizontal gas-liquid pipe flow with low liquid loading

Netaji R. Kesana*, Roberto Ibarra, Morten Langsholt, Roar Skartlien, Olaf Skjæraasen, Murat Tutkun

Department of Process and Fluid Flow Technology, Institute for Energy Technology (IFE), Kjeller 2007, Norway

**Keywords:** Low liquid Loading, LDA, Isokinetic Sampling, Atomization, Velocity Profiles

*Corresponding author
E-mail address: Netaji.Ravikiran.Kesana@ife.no, nrk301@utulsa.edu

## ABSTRACT

New data on streamwise droplet velocity profiles for low liquid loading pipe flows are reported. The fluids used in the experiments are $SF_6$ (gas-phase) and Exxsol D60 (oil-phase). Experiments are conducted in a 10 cm pipe diameter high-pressure (~780 kPa, absolute) flow loop to reproduce gas-condensate field conditions. Instantaneous streamwise velocity data, obtained using the non-intrusive Laser Doppler Anemometry (LDA) technique, are used to calculate mean and root-mean-squared (RMS) local velocities. Asymmetric droplet velocity profiles with respect to the pipe center-line are observed especially for the stratified low atomization flow conditions. However, as the flow momentum increases, the droplet velocity profiles seem to become more symmetric. Also, these data suggest that, irrespective of the conditions studied, the single-phase gas flow characteristics are preserved closer to the top pipe wall. The data from the LDA imply that the bottom pipe half region is highly influenced by the gas-liquid interfacial characteristics. This results in high streamwise turbulence intensity in the region influenced by the interfacial waves (interfacial turbulence). An isokinetic sampling instrument is also used to measure the local instantaneous dynamic pressure. The dynamic pressure and the locally extracted liquid (droplets) volume rate under isokinetic conditions are used to calculate local fluid velocity. Excellent agreement has been obtained when comparing this calculated local velocity from the isokinetic instrument to the LDA data.

# 1. INTRODUCTION

Low liquid loading is a condition in a pipeline where the liquid volumetric flow rate is considerably lower than the gas volumetric flow rate. This is a very common condition present inside gas transportation pipelines. This small quantity of liquid is carried in the form of a liquid film on the pipe wall and droplets dispersed in the gas. The droplets are formed and ejected into the gas phase due to the shear at the gas-liquid interface (Skartlien et al., 2011). These droplets can travel at high velocities compared to the liquid velocity inside the film and thus play a critical role in liquid transportation. It is recognized that the droplet acceleration in the gas space results in a higher pressure drop increase in the system.

Even though the amount of liquid can be extremely small inside the low liquid loading systems, its impact on the pressure drop and further flow assurance challenges such as hydrate formation and top-of-line corrosion can be significant. Additionally, gas transportation flow facilities and collection systems are designed using certain low liquid loading flow models implemented into commercial software. The reliability of the system design is therefore directly affected by the accuracy of these flow models. A more comprehensive understanding of the low liquid loading pipe flows is essential to develop more physical and accurate flow prediction models. One, or perhaps the only, way to achieve this is to carry out carefully designed flow experiments and to understand the underlying processes. The most essential parameters which can shed light on this problem and which can also be extracted through laboratory experiments under low liquid loading flows include pressure drop, liquid hold-up, entrained liquid fraction, film thickness circumferential distribution, wetted fraction, wave characteristics (amplitude and frequency), velocity fields inside the gas phase and liquid film, wall shear stress distribution, and droplet velocity and size distributions. Hereafter parameters other than pressure drop and liquid hold-up are referred to as in-situ flow parameters.

There have been a handful of studies focused on the liquid entrainment inside the gas phase (e.g., Gawas et al., 2013; Magrini et al., 2009; Mantilla et al., 2006; Pan and Hanratty, 2002; Sawant et al., 2008; Tayebi et al., 2000; Vuong et al. 2017; Karami et al. 2017; Kesana et al. 2018). Despite several experimental measurements of liquid entrainment, there still exists a strong need for further quantification of droplet entrainment, especially in high-pressure systems and using an industrially more relevant liquid-phase other than water (Al-Sarkhi et al., 2012). The liquid entrainment mechanism is inherently complex and coupled with several other in-situ local flow parameters like wave characteristics, droplet velocities, and drop size distributions to name a few. A common obstacle in the development of better flow models is the lack of suitable experimental datasets

in the literature, in particular when it comes to in-situ parameters. In many cases, experimental results cover only a very limited parameter range, and are presented in a dimensional form which is nontrivial to generalize.

Notwithstanding this, there are some investigations in the literature studying the gas-liquid interface wave characteristics. The behavior of the interface waves can result in increased interface shear stress and hence pressure drop. Most works on this subject (see, for instance, Andritsos and Hanratty (1987) and Tzotzi and Andritsos (2013)) focused on waves in stratified gas-liquid flows, in the absence of atomization. Yet recently, Gawas et al. (2014) measured wave characteristics (celerity, amplitude, and frequency) on gas-oil interfacial waves under low liquid loading conditions. They found that the wave celerity (the speed of the wave trough/crest) was correlated with the ratio between the liquid and gas Froude numbers. One should note that interfacial wave characteristics influence greatly the droplet generation mechanisms. Typically, the interfacial waves are characterized as disturbance or Kelvin−Helmholtz waves. The effect of fluid properties (viscosity and surface tension) on disturbance wave characteristics has been recently reported by Setyawan et al. (2016).

Two important parameters that influence droplet generation, transportation and possibly deposition mechanisms are the circumferential film thickness and the wall shear stress distribution. There exists no dataset in the literature that includes these parameters for low liquid loading conditions, probably due to difficulties with quantifying thin liquid films. Some works present film thickness measurements in annular flows, but not in low-liquid loading cases (e.g., Alamu and Azzopardi, 2011; Schubring et al., 2010). For example, in a recent study, Schubring et al. (2010) used Planar Laser-Induced Fluorescence (PLIF) measurement technique to visualize the liquid film with rough gas-liquid interface and quantify the statistical information about the film thickness.

This paper presents velocity measurements of the droplets generated possibly due to the action of interfacial shear between the gas phase and the liquid film. The droplets are torn out from the disturbance waves (gas-liquid interfacial waves) and carried by the gas phase. The Laser Doppler Anemometer (LDA) measurement technique is employed to measure local streamwise velocities instantaneously. The time-series are then used to obtain statistical parameters like root-mean-squared or RMS and mean velocities. The only work which we find to be of direct relevance to this study is Paras et al. (1997) where the atomization is very low, i.e., very low liquid entrainment. The experiments presented in our paper focused on not only low atomization case, but also moderate and high atomization cases. One should note that the data presented in this paper is limited to the gas-space region due to practical reasons. Velocity measurements inside the liquid film (and liquid layer characteristics) have turned out to be extremely difficult and therefore not considered in the present study.

Additionally, we present the pressure drop data to emphasize that small quantities of liquid can adversely affect the system at large scale and increase the system pressure drop substantially. The dynamic pressure measurements as documented in the following sections are based on our isokinetic sampling system measurements. A comparison between the local velocities obtained using isokinetic probe and LDA probe is presented in the paper.

# 2. EXPERIMENTAL TECHNIQUE

## 2.1 Flow Facility

Droplet field characterization experiments were performed at the IFE Well Flow Loop (WFL), as presented in Fig. 1. The test section consists of a 45 m long PVC pipe of 10 cm inner diameter and is equipped with several flow measuring instruments. The desired quantities of gas and liquid are injected at the inlet of the test section. From the outlet of the test section facility, the flow mixture is separated (stage-one separation) at the pre-separator. Then, the gas-phase with some liquid carry-over flows to a gas-liquid separator. The separated liquid is directed into a liquid-liquid separator. Note that the flow loop is capable of conducting three-phase experiments; however, the present investigation is restricted to two-phase flow studies. The liquid-liquid separator is also connected to the gas-liquid separator so the liquid carried-over in the gas-liquid separator can drain back into the liquid storage tank (i.e., liquid-liquid separator). In the same way, the remaining gas in the return liquid stream can flow to the gas storage (i.e., gas-liquid separator). The gas from the gas-liquid separator flows to the gas booster via the gas scrubber. The gas scrubber contains a number of mesh pad agglomerators and demisting cyclones to remove the extremely small quantities of liquid present in the gas phase before flowing into the gas compressor as a dry gas.

A major challenge with the low liquid loading experiments is to maintain the superficial liquid velocities with the lowest possible uncertainty. This requires removing any liquid from the gas-phase line and using an accurate liquid flow meter. We have therefore kept the gas scrubber in operation during the campaign, as explained earlier. Furthermore, we used a Coriolis flow meter manufactured by Bronkhorst in order to achieve an accuracy better than ±0.3% of the measured reading. The Coriolis flow meter measures the density and the flow rate of the liquid independently during the experiments as the test liquid is pumped continuously. The gas flow rate is measured using a turbine flow meter, manufactured by Elster-Instromet, which has an accuracy of ±1.5% of the actual volumetric flow. The temperature of both gas and liquid phases is controlled using heat exchangers installed upstream of the inlet section with a target temperature of 20 ± 1 °C. Detailed uncertainty analysis is presented in Section 2.1.2.

During the experiments all flow and operation parameters are monitored continuously using the Supervisory Control and Data Acquisition (SCADA) system. The data from the instrument channels are logged using the average and time-series loggers. The average logger acquires data at a frequency of 0.1 Hz for a period of 60 s. In addition, the data acquisition frequency of the time-series logger is 50 Hz, and data is logged for a period of 100 s.

In this investigation, we have used 5 differential pressure transducers manufactured by Fuji Electric, the in-house built isokinetic sampling equipment (located at $L/D$ ~ 445), and a non-intrusive optical LDA (located at $L/D$ ~ 320) set-up supplied by Dantec Dynamics.

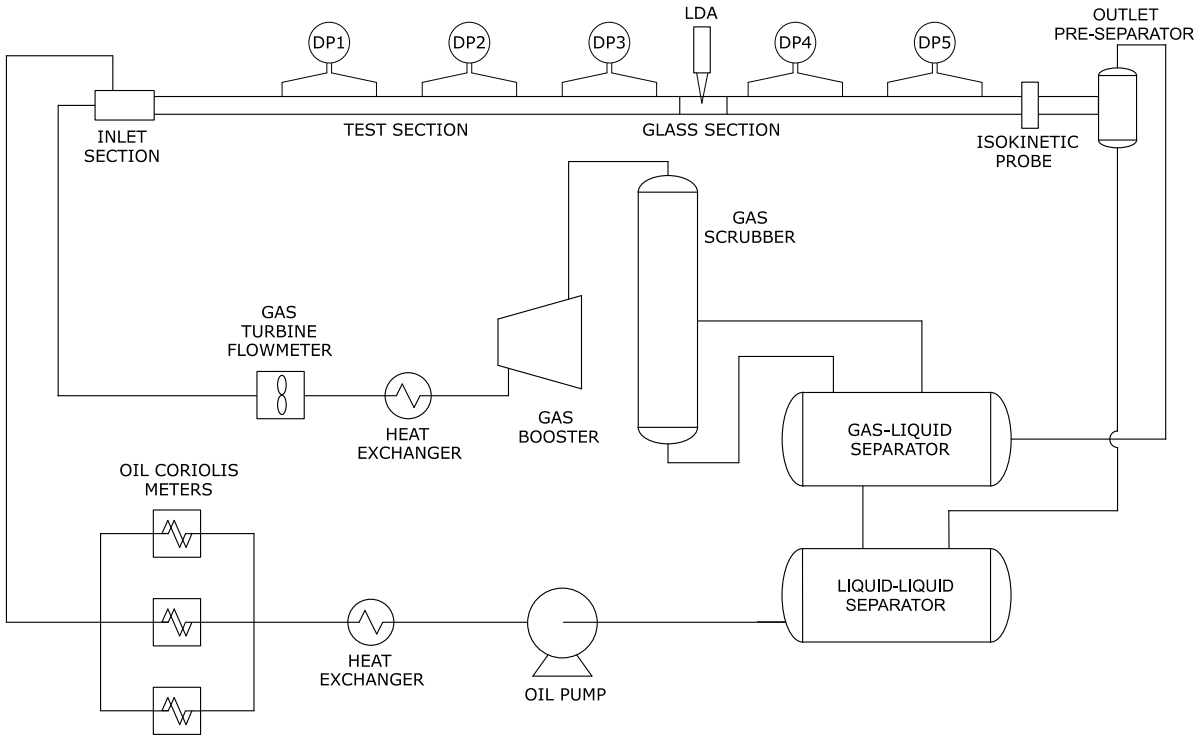


**Fig. 1. Schematic of the test flow loop**

### 2.1.1 Test Matrix

As noted earlier, all the laboratory experiments are conducted in a horizontal test section, with $SF_6$ (gas-phase) and Exxsol D60 (liquid-phase) as the test fluids. The fluid properties are presented in Table 1. The measured surface tension between $SF_6$ and Exxsol D60 at 800 kPa (absolute) pressure is 28.3 mN/m. The gas-liquid surface tension is measured with a Krüss Drop Shape Analyser, Model DSA100B. This instrument allowed us to measure the surface tension for the pressurized fluid samples. During our laboratory studies, the superficial gas velocity is varied from 5 m/s to 10 m/s, whereas the superficial liquid velocity is varied from 1 mm/s to 7 mm/s. These conditions were chosen in order to have an extremely low liquid content inside the system and to have a significant droplet atomization. Table 2 presents the studied experimental cases to quantify droplet velocity statistics. The entrained fraction values for some of the studied conditions are presented in this table. Readers are advised to see Kesana et al. 2018 for the details regarding the droplet entrainment quantification measurements. In the next sections, a description of the major instruments used in the current investigation (Laser Doppler Anemometer and Isokinetic Sampling Probe) is given.

**Table 1.** Fluid properties at 800 kPa (absolute) and 20°C

| Fluid | Density ($kg/m^3$) | Viscosity ($Ns/m^2$) × $10^{-3}$ |
|---|---|---|
| $SF_6$ | 51 | 0.015 |
| Exxsol D60 | 815 | 1.41 |

**Table 2.** Experimental conditions for LDA measurements. Stratified wavy flow regime represents incomplete or partial pipe wall wetting, and annular represents the pipe wall completely wetted with liquid. Droplet entrained fraction in the gas space is quantified using the isokinetic sampling instrument.

| $U_{SG}$ (m/s) | $U_{SL}$ (mm/s) | $f_E$ (%) | Flow regime |
|---|---|---|---|
| 5 | 1 | 7.8 | Stratified wavy |
| 5 | 3 | 4.5 | Stratified wavy |
| 5 | 5 | 5.8 | Stratified wavy |
| 5 | 7 | 2.7 | Stratified wavy |
| 6 | 1 | - | Annular |
| 7 | 1 | - | Annular |
| 7.5 | 1 | 56.5 | Annular |
| 8 | 1 | - | Annular |
| 10 | 1 | 66.5 | Annular |

### 2.1.2 Uncertainty Analysis

Detailed uncertainty evaluations of the instruments and measurements are reported in this section. The total measurement error is a combination of random and systematic errors. When reporting the uncertainty, both the random and systematic uncertainty components are accounted for. The random standard uncertainty is calculated from the standard deviation of the measurements obtained from the time-series data (repetitions of measurements). Systematic uncertainty is the difference between average measured values and a known (true) value, which is generally estimated from the accuracy of the instrument provided with the equipment datasheet. Table 3 presents the uncertainty estimates for geometry, fluid and flow parameters. The stated values are conservative estimates, as the uncertainty of many parameters changes with each experimental condition.

The pipe sections in the WFL are made of PVC. Several diameter measurements have been made at different sections of the PVC pipes to estimate the random uncertainty. A caliper, with an accuracy of 0.01 mm, is used to estimate the systematic uncertainty component. Furthermore, the pipe inclination is carefully adjusted using a laser distance measure meter. The deviations in the elevation measurements over several beam lengths are

used to estimate the measurement uncertainty in the pipe inclination. The gas density is measured from weighing the gas in the pycnometer. The uncertainty in the volume of the pycnometer and the scale readings are considered to estimate the measurement uncertainty of gas density. The uncertainty in the oil density is estimated from the accuracy of the Coriolis flow meter and the time-series density measurements. The gas and liquid viscosity measurements are function of the system temperature. However, two heat exchangers are incorporated to have a negligible fluid temperature variation at the inlet section. The reported uncertainty value in the gas viscosity is estimated from the functional relationship between gas viscosity and temperature. Typically, the gas viscosity increases with the square of temperature. To estimate the liquid viscosity, the liquid viscosity measurements are performed using an Anton Paar MCR 301 rheometer at different liquid temperatures. Then, the functional expression between the liquid viscosity and the temperature is used to estimate the uncertainty in liquid viscosity.

In order to estimate the uncertainty in the superficial gas and liquid velocities, the uncertainty propagation analysis is performed. For example, the uncertainty in superficial gas velocity will account for the total uncertainties in system pressure, temperature, gas mass flow rate, and pipe diameter. This method of estimating error propagation is based on Taylor series expansion, which is commonly used in areas of thermos-fluids (for example, see Sheikholeslami and Ganji 2016).

**Table 3.** Overview of the uncertainty measurements.

| **Parameter** | **Symbol** | **Measurement Uncertainty** | **Absolute/Relative** |
|---|---|---|---|

| | | | |
|---|---|---|---|
| Pipe diameter, mm | $D$ | ±0.17 | Absolute |
| Pipe inclination, ° | $\theta$ | ±0.03 | Absolute |
| Gas density, kg/m$^3$ | $\rho_G$ | ±2.4 % | Relative |
| Oil density, kg/m$^3$ | $\rho_L$ | ±0.3 % | Relative |
| Gas viscosity, mPa s | $\mu_G$ | ±6.7 % | Relative |
| Oil viscosity, mPa s | $\mu_L$ | ±2 % | Relative |
| Surface tension, mN/m | $\sigma$ | ±5 % | Relative |
| Absolute pressure, bar | $P$ | ±2 % | Relative |
| Temperature, °C | $T$ | ±1 | Absolute |
| Superficial gas velocity, m/s | $U_{SG}$ | ±3.5 % | Relative |
| Superficial liquid velocity, m/s | $U_{SL}$ | ±2.7 % | Relative |

### 2.2 Laser Doppler Anemometer

The LDA non-intrusive measuring technique is used to obtain the streamwise velocities of the droplets in the two-phase low liquid loading system. From the instantaneous readings, the time-averaged mean and RMS velocities are calculated.

For the current study we have used the 2D-LDA system developed and supplied by Dantec Dynamics. The laser beam (at 488 nm with a 1000 mW Argon-Ion laser source) is split to achieve the frequency shift of 40 MHz using the transmitting optics (Bragg cell). Then these two coherent blue laser beams are focused onto a 160-mm focal length lens and intersected to form an ellipsoidal measurement volume. The diameter of the focused laser beam is 75 µm with a beam intersection angle of 0.24 rad. As a result, the diameter and length of the measurement volume are 76 µm and 0.64 mm, respectively. This measurement volume is composed of bright and dark fringes. The formation of these fringes is due to the interference of the light waves. Once the particle (droplet) passes through the measurement volume, the intensity of the backscattered light fluctuates with a frequency equal to the droplet velocity divided by the fringe spacing (2.07 µm). This scattered light is gathered at the photomultiplier (receiver). The signal from the photomultiplier is sent into signal conditioner and then into the counter signal processor for further analysis.

The precise spatial movement of the LDA's measurement volume from the top pipe wall towards the bottom of the pipe (near to the gas-liquid interface) is performed by a traverse system. The laser probe is fixed to

an adjustable arm which can make precise movements in the three-dimensional space. The traverse system is integrated with a BSA (Burst Spectrum Analyzer) software and the measurements are made sequentially. It is important to mention that during the present study, we did not use any seeding particles, instead we used the droplets to measure velocities as they pass through the LDA measurement volume. One should note that any particle or any other agent used as seeding particle may change the gas-liquid interface characteristics significantly (Ayati et al. 2014).

Velocity measurements were performed in a short borosilicate glass section ($L/D$ = 40), with a thickness of 10 mm, located at $L/D$ = 320 from the inlet. The initial position of the measurement volume (the laser beam intersection) was set at the top region of the pipe taking into account the light refraction at the inner and outer pipe wall as showed in Fig. 2. The angle of refraction at the inner and outer pipe wall is constant as the traverse system travels towards the bottom of the pipe because both laser beams are located in the vertical plane that passes through the center-line of the pipe. The vertical position of each measurement point ($y$), after refraction, corresponds to the same position from the traverse system, from the initial calibration at the top of the pipe, as the refractive indices of the outside fluid (air) and inside fluid ($SF_6$) are the same ($\eta$ = 1).

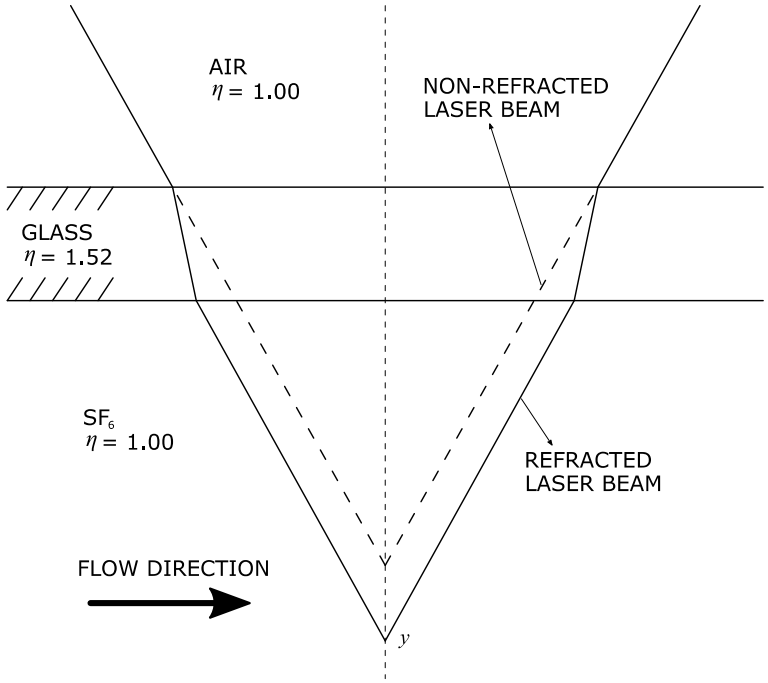


**Fig. 2. LDA laser beams configuration**

### 2.3 Isokinetic Sampling System

The isokinetic system consists of a sampling tube of diameter 3.2 mm which can be positioned at any location along the vertical pipe diameter. During each experiment, the droplet volume is extracted into a cylinder in an isokinetic manner. This means that the sample extraction rate is controlled until the differential pressure between the probe inlet and the wall static pressure approaches zero. By this we reduce the influence of diverging streamlines around the probe tip and therefore we extract approximately representative fluid samples. The original purpose of this device is to measure the liquid entrainment fraction, which is defined as the ratio of droplet mass flow rate to the liquid mass flow rate. We show in this study that isokinetic probes can also be used to estimate the local droplet velocities by measuring the local dynamic pressure. This can be done after setting the probe at isokinetic condition and completely closing the valve regulating the liquid flow rate into the cylinder, and then the differential pressure readings suggest the dynamic pressure at the probe tip. Dynamic pressure is the result of the droplet flow rate and the local concentration. Typically, the higher the droplet flow rate is the greater the local dynamic pressure. The combined measurements of droplet volume flow rate and the time-averaged dynamic pressure can be used to calculate the local mean velocity of the droplets. It is worth pointing out that the extraction of representative liquid volume is dependent on the probe tip location inside the pipe and the flow conditions. For example, during the present investigation of low liquid loading and low entrained fraction conditions, the time to extract the representative volume of liquid closer to the top pipe wall took approximately around 70 minutes. The readers are referred to the Tayebi et al., 2000 and Kesana et al., 2018 for further details about the isokinetic sampling instrument construction.

## 3. RESULTS AND DISCUSSION

In this section, pressure drop data are first presented, showing the importance of low liquid loading flow studies. Then, velocity data and LDA measurements close to the top pipe wall are presented. This is followed by a presentation of the mean and turbulent intensity velocity profiles for several experimental cases. Then, the dynamic pressure and the calculated local droplet velocity measurement using the isokinetic sampling techniques are presented. Finally, a comparison of the mean velocity data from the LDA and isokinetic sampling techniques is given.

### 3.1 Effect of small quantities of liquid on the pressure drop

Pressure gradients have been measured for low liquid loading two-phase flow, as well as for single-phase gas flow. The relative increase of the pressure drop due to the presence of liquid is given by,

$$\nabla P_{\text{rel}} = \left( \frac{\left(\frac{dp}{dL}\right)_{\text{TP}} - \left(\frac{dp}{dL}\right)_{\text{SG}}}{\left(\frac{dp}{dL}\right)_{\text{SG}}} \right) \quad \text{(Error! Bookmark not defined.1)}$$

where $\left(\frac{dp}{dL}\right)_{TP}$ is the pressure gradient for the two-phase low liquid loading experiment, and $\left(\frac{dp}{dL}\right)_{SG}$ is the pressure gradient for single-phase gas flow.

Fig. 3 shows the behavior of $\nabla P_{\text{rel}}$ as the superficial liquid velocity, $U_{\text{SL}}$, increases for a given superficial gas velocity, $U_{\text{SG}}$. These experiments were performed with $U_{\text{SL}}$ values of 1, 3 and 5 mm/s. This corresponds to liquid loading values of 4.3, 12.8, and 21.3 Stb/d (standard barrels per day). The addition of these small quantities of liquid resulted in significant increase in the system pressure drop. The maximum increase is approximately 85 % when $U_{\text{SL}}$ and $U_{\text{SG}}$ are equal to 5 mm/s and ~8 m/s respectively.

The relative increase in the pressure drop is a function of both $U_{\text{SL}}$ and $U_{\text{SG}}$. It is higher when there is more liquid in the system (with exception of $U_{\text{SG}}$ = 14 m/s and $U_{\text{SL}}$ = 1 mm/s). In all the cases studied herein, $\nabla P_{\text{rel}}$ increases with $U_{\text{SG}}$, up to a critical value. Thereafter, $\nabla P_{\text{rel}}$ remains almost constant as $U_{\text{SG}}$ increases further. For $U_{\text{SL}}$ = 1 mm/s, further increase in pressure drop is observed after the plateau is reached at higher superficial gas velocities. Unfortunately, it is not possible to discern from these data exactly how the different mechanisms contribute to $\nabla P_{\text{rel}}$ after the plateau. The flow involves a combination of rather complex mechanisms such as wave breakup, droplet entrainment and deposition, interfacial turbulent stresses, and film turbulence. Here, it should be emphasized that extremely small amounts of liquid in the system can potentially lead to large increases in energy consumption for the gas transportation installations. It should be recalled from Section 1 that the major goal of this study is related to the instantaneous and time-averaged droplet velocity measurements.

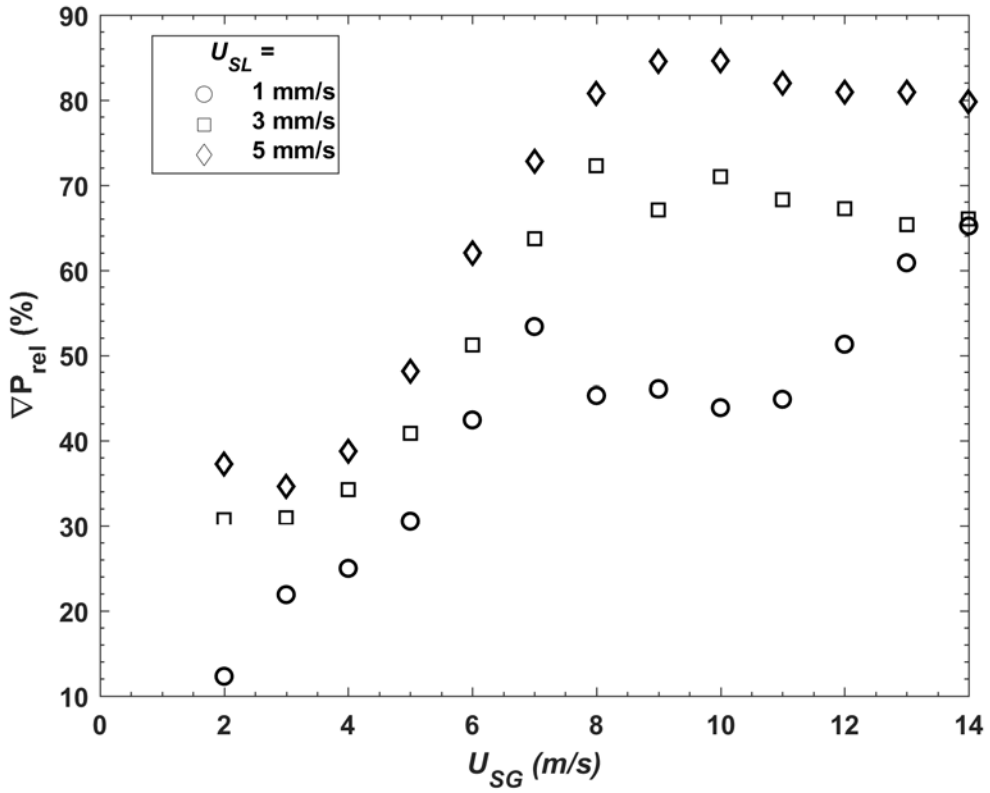


**Fig. 3.** Effect of superficial gas and liquid velocities on percentage pressure drop increase for low liquid loading flows.

### 3.2 Instantaneous velocity measurements and near top-wall velocity characteristics

The pressure drop data, as presented in previous sections, revealed the importance of fundamental understating in low liquid loading flows. The instantaneous streamwise droplet velocity is measured in the gas space at closely located measurement points along the vertical axis of symmetry. During the measurements, the LDA data acquisition rate varied depending on the local mean droplet velocity and the position of the laser beam with respect to the wall. In order to ensure good statistical convergence at least 2000 statistically uncorrelated, independent samples are acquired for each experimental run. Fig. 4 illustrates two typical LDA velocity readings: one near the top wall, $y$ = 5 mm, and one at the pipe–center, $y$ = 50 mm ($y$ = 0 corresponds to the top pipe wall). As expected, velocity fluctuations closer to top pipe wall are much larger compared to those observed at the pipe-center.

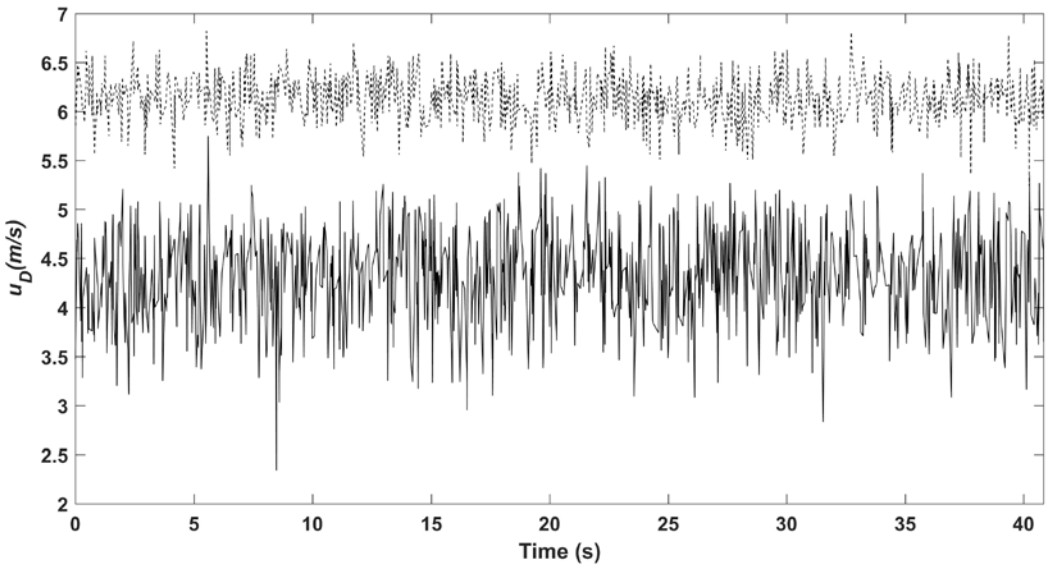


**Fig. 4.** Time-evolution of streamwise droplet velocity measurements when $U_{SG}$ = 5 m/s, $U_{SL}$ =1 mm/s. Solid and dashed lines correspond to the velocity measurements at $y$ = 5 and 50 mm, respectively.

The cases with $U_{SG}$ = 5 m/s are studied first, because at this gas velocity there exists only a small amount of droplets, and the top pipe wall is not wetted with liquid. This is a typical stratified-wavy pipe flow case with inadequate droplet atomization to create complete pipe wall wetting. Therefore, we have approximated the gas-to-pipe wall shear using the Tzotzi and Andritsos (2013) stratified flow model, in which the gas-liquid interface friction factor depends on the type of the interfacial waves (2D or 3D). According to Tzotzi and Andritsos, 2D waves are defined as small amplitude periodic waves, while 3D waves are irregular and large amplitude waves. The gas-to-pipe wall shear is used to approximate the friction velocity, $u_\tau$. Since the liquid loading is very small in this investigation, we also estimated the wall shear stress close to the top pipe wall using the Haaland equation in case of a single phase flow. Table 4 tabulates the gas-to-wall shear stress and friction velocity calculations using both methods. The difference in the calculated friction velocities between these two methods is very small because of extremely low liquid holdup. One should note that at the top wall, there is essentially no difference between single phase flow and two-phase flow, with respect to either the shear stress or $u_\tau$. Similarly, there is a negligible difference in the calculated shear stress between different $U_{SL}$ values in this study, when $U_{SG}$ is kept constant. On the other hand, we have observed a large difference in pressure drop values at different liquid rates when compared with single phase gas flow or each other. Considering the fact that the pressure gradient in the vertical direction is zero, most of the pressure drop is caused by the interfacial stress at the gas-liquid interface. Depending on the liquid flow rate, characteristics of the interface can vary substantially, as has been indicated by the large differences in pressure drop values presented in Fig. 3.

**Table 4.** Gas-to-wall shear stress calculated from Tzotzi and Andritsos (2013) stratified flow model. $U_{SG}$ = 5 m/s. Flow pattern = stratified-wavy with small amount of droplets. Shear stress and the friction velocity calculated using single phase approach are $\tau_{w\,(1\text{-phase})}$ = 1.67 N/m$^2$ and $u_\tau$ = 0.187 m/s.

| $U_{SL}$ (mm/s) | $\tau_{w(2\text{-phase})}$ (N/m$^2$) | $u_\tau$ (m/s) |
|---|---|---|
| 0 | - | 0.187 |
| 1 | 1.59 | 0.183 |
| 3 | 1.60 | 0.183 |
| 5 | 1.61 | 0.184 |
| 7 | 1.62 | 0.184 |

The wall friction velocity is then used to calculate the inner scaling parameters ($y^+$ and $u^+$). Here, $u_\tau = \sqrt{\frac{\tau_w}{\rho}}$, $y^+ = \frac{y u_\tau}{\upsilon}$, and $u^+ = \frac{<u_x>}{u_\tau}$. The mean axial velocity, $< u_x >$, is defined as,

$$< u_x >= \frac{1}{n}\sum_{i=1}^{n} u_{D,i} \tag{2}$$

where n is the number of samples and $u_{D,i}$ is the instantaneous axial velocity measurement. A number of studies of single-phase wall-bounded turbulent flows have shown the existence of the inertial sublayer, where the scaled local mean velocity ($u^+$) follows a logarithmic distribution with the scaled distance ($y^+$) away from the pipe wall,

$$u^+ = \frac{1}{\kappa}\ln y^+ + A \tag{3}$$

where $\kappa$ and $A$ are the Von Kármán constant and a constant which depends on surface roughness, respectively. According to Bailey et al. (2014), five different high Reynolds number (turbulent flows) datasets in a hydraulically smooth pipe ranging from Reynolds number of $81 \times 10^3$ to $1.8 \times 10^7$ indicated Von Kármán constant ($\kappa$) of ~ 0.4.

Therefore, in our analysis $\kappa$ is set to be 0.4, while we treat $A$ as a variable to be found via regression analysis of the data. Fig. 5 shows a semi-log plot of streamwise velocities for all the superficial liquid velocity cases (1 to 7 mm/s) and a superficial gas Reynolds number, $Re_{SG} = \frac{\rho_G U_{SG} D}{\mu_G}$, fixed at $1.6 \times 10^6$. The superficial liquid Reynolds number, $Re_{SL} = \frac{\rho_L U_{SL} D}{\mu_L}$, is varied from 58 to 405. The friction velocity which we used to scale the wall-normal position and the mean velocity is calculated using the two-phase flow model described earlier. The solid straight lines in each of the plot in Fig. 5 correspond to the best data fit to the available data. The dashed lines, on the other hand, present the classical single phase smooth pipe flow profile when κ=0.4 and $A$=5.5.

As seen from Fig. 5, the LDA measurements start inside the inertial layer due to practical difficulties in the vicinity of the wall. These difficulties are more pronounced for the case (a) presented in Fig. 5, with $U_{SL}$ = 1 mm/s. For all other cases, the data follow the logarithmic profile inside the inertial region and depart from the logarithmic line as the flow is above the inertial region into the wake region. It should be noted that even if we used the friction velocity obtained using the single phase approach, the results will not vary greatly (see Table 4). The reason for retaining the single-phase behavior closer to the top pipe wall is not having a fully wetted top-wall, and droplets being very small. These droplets just follow the gas stream without changing the flow characteristics. In other words, there is negligible slippage between the gas phase and these small droplets. Therefore, the mean axial droplet velocity close to the top pipe wall should be representative of the mean axial gas velocity. Furthermore, the local droplet concentration is very small in the regions closer to the top pipe wall (in the upper pipe half region).

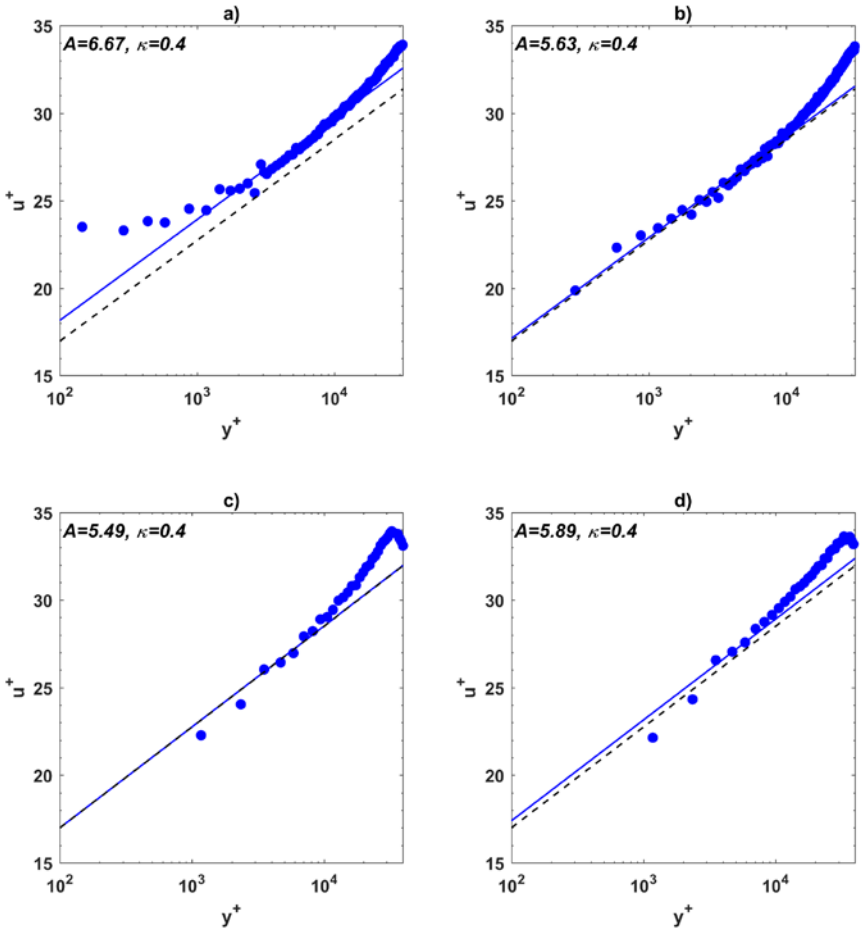


**Fig. 5.** Streamwise mean droplet velocity profile near the top pipe wall. $U_{SG}$ = 5 m/s, $Re_{SG}$ = 1.6 x $10^6$. a) $U_{SL}$ = 1 mm/s, $Re_{SL}$ = 58. b) $U_{SL}$ = 3 mm/s, $Re_{SL}$ = 173. c) $U_{SL}$ = 5 mm/s, $Re_{SL}$ = 289. d) $U_{SL}$ = 7 mm/s, $Re_{SL}$ = 405. The solid and dashed lines correspond to equation, $u^+ = \frac{1}{\kappa}\ln y^+ + A$ . The values of $\kappa$ and $A$ are shown in

the figure for the solid lines. For the dashed lines the values of $\kappa$ = 0.4 and $A$ = 5.5. See Table 2 for the entrained fraction values.

At high gas velocities, it is possible to visually observe the formation of a liquid film at the top pipe wall even though it is extremely thin and difficult to quantify. The entire pipe circumference can therefore be considered wetted by the liquid film under these conditions. As shown in Fig. 5, the axial velocity data closer to the top pipe wall follow the single-phase dimensionless logarithmic expression, in particular within the inertial layer. To generate the inner scaling parameters, i.e., to normalize velocity and wall-normal distance in Fig. 5, we used both two-phase and single-phase models to estimate friction velocity. However, the application of Tzotzi and Andritsos two-phase model for highly atomized flows with complete wall wetting is not justifiable, as this model was developed for stratified smooth and wavy interface flows with no atomization.

In order to calculate the friction factor, $U_{SG}$ is used as the bulk velocity in the pipe, and this is incorporated into the single-phase flow relations. Since the liquid film is very thin, it is a reasonable assumption to use the shear stress estimated from the single phase flow approach. With this assumption, Fig. 6 shows the local axial mean velocity profiles in terms of inner parameters for $U_{SG}$ values ranging from 5 m/s to 10 m/s at a constant $U_{SL}$ of 1 mm/s. The solid straight line shown in the figure is the well-known logarithmic velocity profile for the single phase turbulent flows in a smooth pipe, Eq. (3) with $\kappa$ = 0.4 and $A$ = 5.5. Most data follow the single phase flow dimensionless logarithmic expression with small deviations which can be attributed to the errors associated with the estimation of wall shear stress, and thus friction velocity. These errors should be small because of the very large gas mass flow rate in comparison with the liquid mass flowrate. Thus, applying single-phase flow correlations/expressions to calculate the wall friction is justifiable. From Fig. 6, it can be concluded that the single-phase theory is valid closer to the top pipe wall for the low liquid loading flows irrespective of the amount of atomization. Note that at the higher gas velocities, there will be a larger amount of atomization.

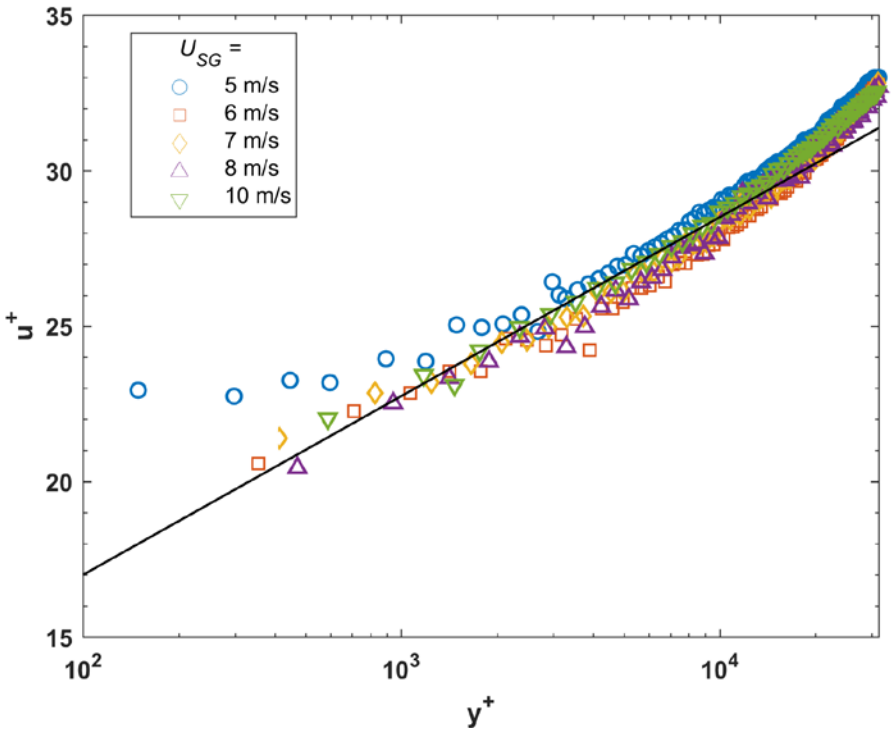


**Fig. 6.** Streamwise mean droplet velocity profile near the top pipe wall. $Re_{SG}$ = 1.6 x $10^6$ - 3.3 x $10^6$, $U_{SL}$ = 1 mm/s. The solid straight line correspond to the equation $u^+ = \frac{1}{\kappa}\ln y^+ + A$, with κ = 0.4 and $A$ = 5.5. See Table 2 for the entrained fraction values.

Fig. 7 compares the mean velocity profiles at two different Reynolds numbers based on pipe radius and friction velocity ($R^+ = \frac{Ru_\tau}{\upsilon}$). The data agree well, in particular within the inertial range. Even though the range of Reynolds numbers tested in this study is very limited, doubling the Reynolds number just expanded the inertial layer as seen in Fig 7. This data further show the single-phase gas flow characteristics are preserved near the top pipe wall.

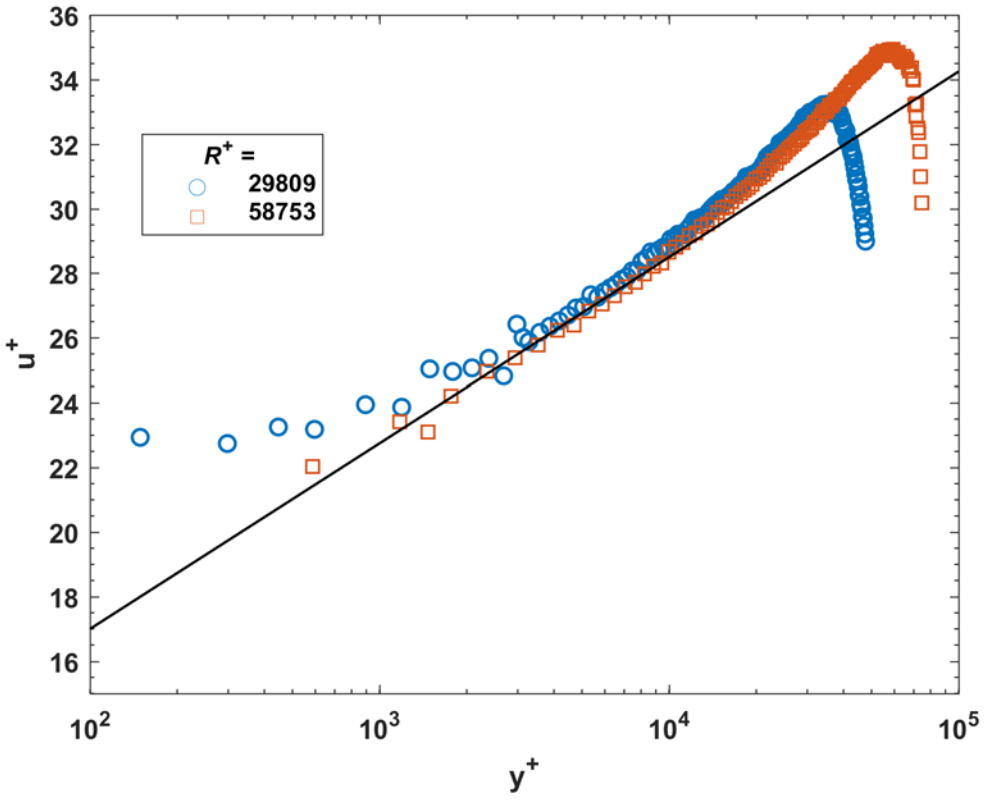


**Fig. 7.** Normalized mean velocity profiles showing the influence of scaled pipe radius ($R^+$). The solid straight line corresponds to equation, $u^+ = \frac{1}{\kappa}\ln y^+ + A$, with $\kappa = 0.4$ and $A = 5.5$.

### 3.3 Measurement of droplet characteristics: Mean velocity and turbulence intensity

Fig. 8 presents the mean velocity profile data for various $U_{SG}$ values, with $U_{SL}$ kept fixed at 1 mm/s. We should mention again that the LDA probe is traversed from the top wall; the wall-normal distance at the top pipe wall was set to zero along the vertical axis. The measurements were conducted from top wall to the liquid film (i.e., to the gas-liquid interface) near the bottom wall. It has been observed that light reflections are highest inside the regions of high droplet concentration. High concentration of droplets indicates high liquid entrainment. As expected, high concentration of droplets corresponds to the region in close proximity to the gas-liquid interface. The height of the droplet dense region depends strongly on $U_{SG}$. When there exists a dense population of droplets, caution must be observed to avoid spurious LDA data, mainly due to strong light reflection from larger droplets, and the presence of the gas-liquid interface.

From Fig. 8, it is observed that the mean droplet velocity profiles are asymmetric. Note that it was not possible to measure half of the profile due to very dense population of the droplets (high local droplet concentration) for the case where $U_{SG}$ is 10 m/s. The main parameter that could influence this behavior is the asymmetric distribution of the liquid film, which is much thinner or not present at the top wall. This also directly influences the inferred size of the droplets and population, especially near the interface. Notice also that the

maximum velocity position is offset from the pipe center-line as marked by the small solid line on each velocity profile in Fig. 8. This offset is more prominent when the superficial gas velocity is 5 m/s, which is the lowest velocity case in this study. The level of atomization depends on the gas velocity, and is minimal at $U_{SG}$ = 5 m/s. The location of the peak velocity moves toward the pipe center-line as increasing the superficial gas velocity. Therefore, a more uniform (symmetric) velocity profile is observed for the case where the superficial gas velocity was 10 m/s. A homogeneous mixture condition inside the pipe at high gas velocity certainly helps to create a more symmetric profile. The turbulence intensity in the gas phase, as well as $Re_{SG}$, increase as $U_{SG}$ increases. Turbulence stimulates the break-up process and creates smaller droplets which are easier to transport and disperse, which then leads to a more homogenous distribution across the pipe cross section.

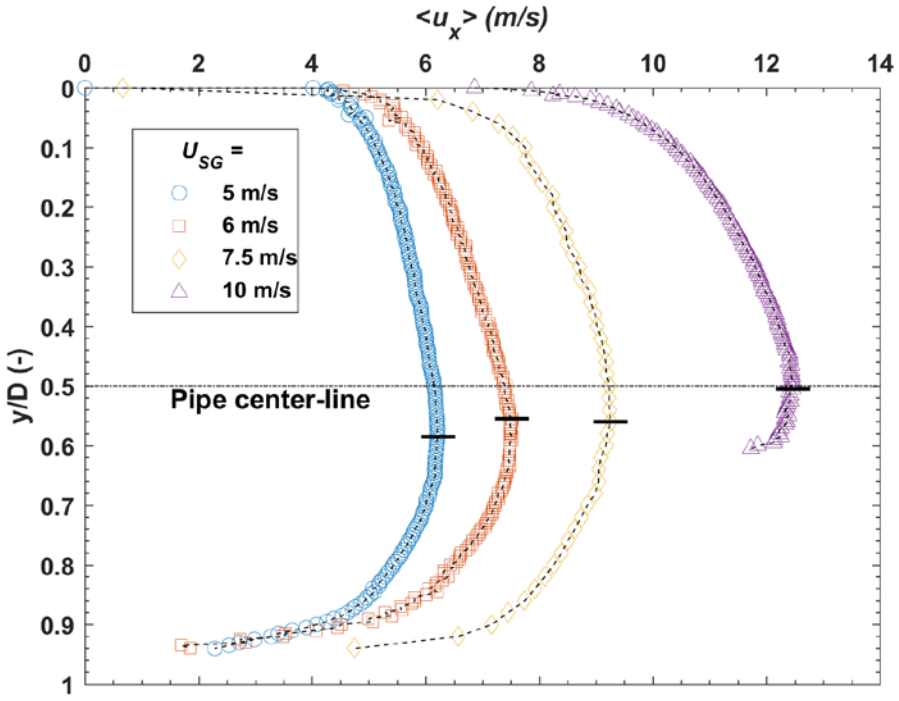


**Fig. 8.** Droplet mean velocity distribution; $U_{SL}$ = 1 mm/s. See Table 2 for the entrained fraction values.

The streamwise turbulent intensity profile data is presented next, for the same flow conditions as in Fig. 9. The streamwise turbulent intensity is defined as the ratio of RMS to mean velocity as described below:

$$I_x = \frac{u_{rms}}{< u_x >} \times 100 \tag{3}$$

$$u_{rms} = \sqrt{\frac{1}{n-1}\sum_{i=1}^{n}\left(u_{D,i} - < u_x >\right)} \tag{4}$$

where $u_{\mathrm{rms},}$ $I_{\mathrm{x}}$ means RMS velocity and turbulence intensity, respectively. Fig. 9 shows the streamwise turbulent intensity profiles for all cases tested in this study when $U_{\mathrm{SL}}$ = 1 mm/s. A closer study of this plot reveals the high turbulence intensity close to the top pipe wall. However, the turbulence intensity values are highest (values are as high as 80%) in the vicinity of the wavy gas-liquid interface region. In this region, the turbulent gas phase shears off the slowly moving liquid from the film to generate droplets. These droplets may deposit back or be carried along with the gas phase. This is also a region with high droplet deposition rate per unit circumferential length attributed to gravitational settling, which further increases the turbulence level. Typically, this region is characterized by the amplitude and frequency of the interfacial waves. The influence of this gas-liquid interface region should also be extended inside the liquid film region. However, to properly quantify the liquid film region, it would be ideal to traverse the laser beam from the bottom wall of the pipe. In this study, since the focus is on phenomena in the gas space, and the liquid film region is not studied. This plot also shows that the streamwise turbulence intensity profiles collapsed to a generic trend (except closer to the interface and below the pipe center-line for $U_{\mathrm{SG}}$ = 10 m/s). For high gas phase Reynolds numbers and high atomization cases, the curves seem to deviate after the pipe center-line.

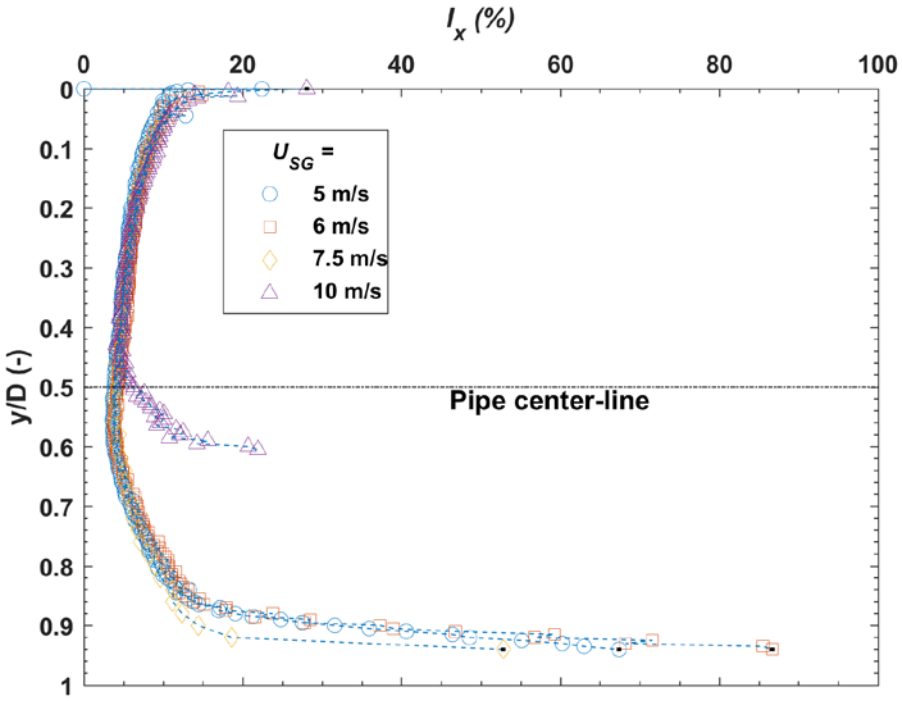


**Fig. 9.** Streamwise turbulent intensity profiles; $U_{\mathrm{SL}}$ = 1 mm/s.

### 3.4 Dynamic pressure measurements and streamwise droplet velocity calculation from the isokinetic sampling

The dynamic pressure is measured at various locations along the vertical pipe diameter intrusively using the isokinetic sampling tube. The variation of the dynamic pressure at different superficial gas velocity conditions is presented in Fig. 10. Similar to the mean velocity data from the LDA experiments as shown in Fig. 8, the dynamic pressure data from the isokinetic probe show asymmetric behavior for superficial gas velocities of 5 m/s and 7.5 m/s. A near-symmetric dynamic pressure profile is observed for the superficial gas velocity of 10 m/s.

It is assumed that the dynamic pressure is equal to the kinetic energy (per unit mass) of the two-phase gas-liquid mixture based on the mixture density ($\rho_M$) and the local mean streamwise mixture velocity ($< u_x >$). This approach was implemented earlier by Skartlien et al. 2011. They obtained the local velocity by solving the equations,

$$P_D = \frac{1}{2}\rho_M < u_x >^2 \quad \text{(Error! Bookmark not defined.5)}$$

$$\rho_M = C_L\rho_L + (1 - C_L)\rho_G. \quad \text{(Error! Bookmark not defined.6)}$$

Here, $P_D$ and $C_L$ are the dynamic pressure and the local droplet concentration, respectively, and the latter is given in terms of the flux and the mean velocity as $C_L = \frac{q_D}{<u_x>}$. Eqs. (5) and (6) can be solved for $< u_x >$ at different measurement locations along the vertical pipe diameter.

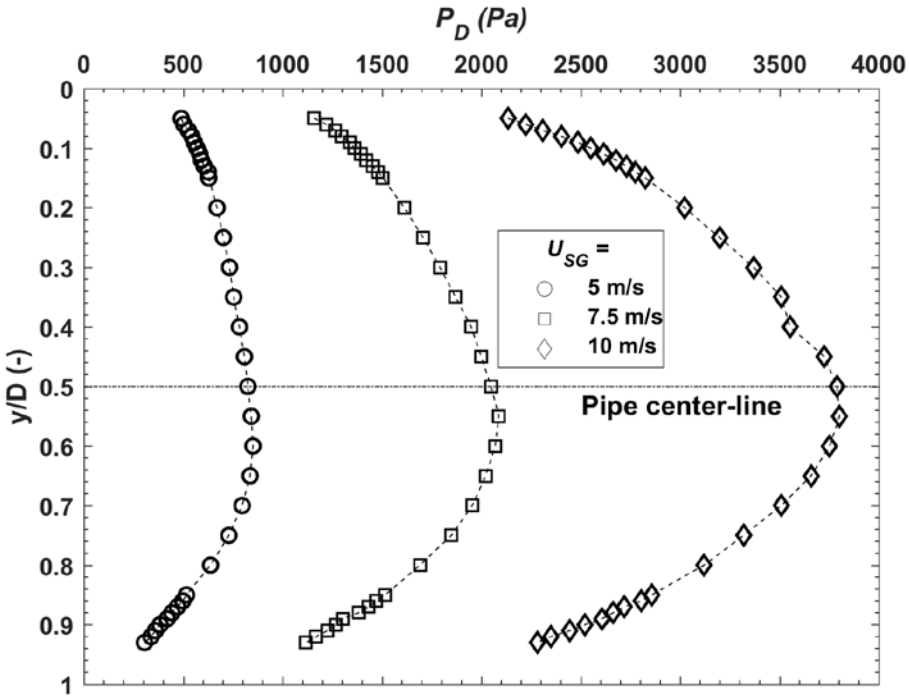


**Fig. 10.** Streamwise mean dynamic pressure profiles along the vertical pipe diameter. $U_{SL}$ = 1 mm/s.

To calculate the mixture density, the volumetric flow rate of the droplets at a specific location is needed (see Eq. 6). Fig. 11 presents the droplet volumetric flow profile along the vertical pipe diameter. The droplet volume is collected under isokinetic conditions at the locations specified in the figure. As expected, the volume fraction of droplets entrained into the gas increases with $U_{SG}$ for a given wall-normal position and $U_{SL}$ value. At low gas velocity, $U_{SG}$=5 m/s, the droplet volume entrained above the pipe center-line, in particular near the top pipe wall, is very small. Using the information of droplet volume rate and the dynamic pressure, Eqs. (5) and (6) are simultaneously solved to obtain the local velocity.

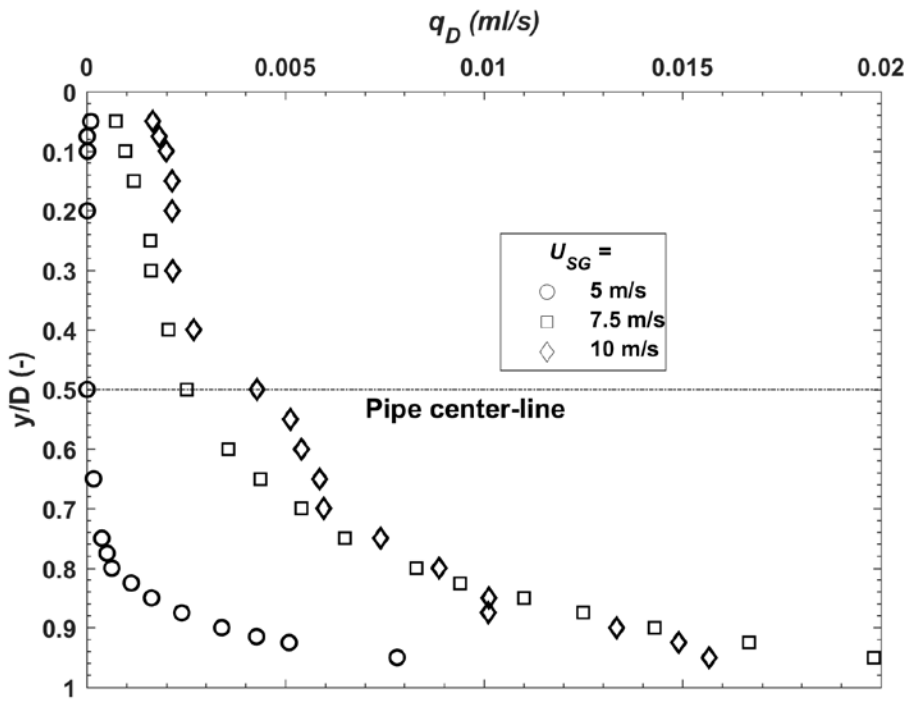


**Fig. 11.** Droplet concentration profiles. $U_{SL}$ = 1 mm/s. See Table 2 for the entrained fraction values.

Fig. 12 shows a comparison between the droplet velocity as measured using LDA and isokinetic probing. Note that the LDA is a non-intrusive technique, whereas the isokinetic measurements are carried out using an intrusive probe with a diameter of 3.2 mm. In order to make LDA and isokinetic probe data comparable, the LDA data are window averaged over a wall-normal distance of 3.2 mm. As seen from Fig. 12, a good match between the isokinetic and LDA measurements is observed for all cases. It should be noted that the isokinetic measurements contain a higher level of noise at high gas velocities (i.e., 10 m/s). This can be attributed to higher pressure fluctuations. Error introduced by this type of noise can certainly be reduced by longer data readings at a given location. Fig. 12 also shows measurement data from the isokinetic probe where LDA did not function properly due to strong reflections. In short, several features about the droplet field (concentration and velocity) can be obtained with the implementation of the isokinetic sampling technique.

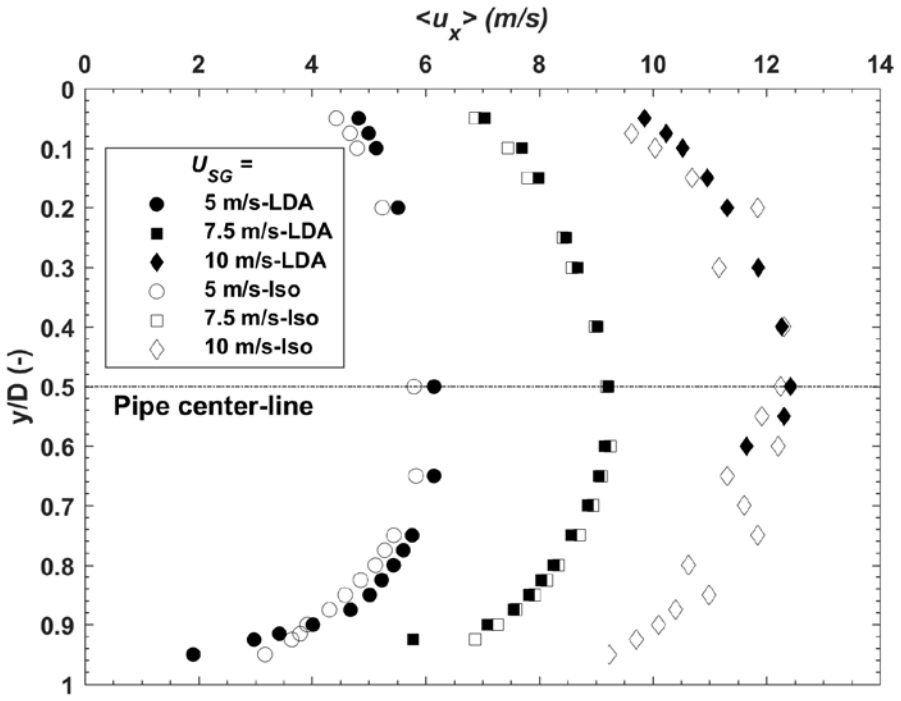


**Fig. 12.** Comparison of streamwise mean droplet velocity measurements (LDA vs. isokinetic). $U_{SL}$ = 1 mm/s. See Table 2 for the entrained fraction values.

### 3.5 Droplet velocity field normalization

It is of interest to check whether the self-similarity exists for the droplet velocity field. In pursuit of finding a common normalization factor for all the experimental conditions, we have extracted the maximum velocity value from each studied LDA droplet velocity profile, respectively. Table 5 summarizes all the droplet velocity measurements performed using the LDA technique, together with the maximum mean droplet velocity values. From this table, one can observe that the ratio of the maximum droplet velocity to the gas superficial velocity is approximately equal to 1.2. The $U_{SG}$ value at the location of the LDA system is used here for normalization. The superficial gas velocity will increase slightly due to the gas expansion (related to the pressure drop) from the pipe inlet to the position of the LDA system. In Table 5 the following table, correction of the gas density is accounted for the calculation of the precise $U_{SG}$ value close to the LDA system. It is important to mention that until this point in this paper, all superficial velocities referred to are based on pipe inlet conditions. Fig. 13 shows this normalized velocity profiles for all the studied conditions. The normalized droplet velocity data very nearly collapsed onto a single curve, indicating a self-similar behavior regardless of atomization conditions.

**Table 5.** Summary of the maximum measured droplet velocity from the LDA technique.

| $U_{SG,\,@Inlet}$ (m/s) | $U_{SG,\,@LDA}$ (m/s) | $U_{SL}$ (mm/s) | $< u_x > \vert_{max}$(m/s) | $\frac{< u_x > \vert_{max}}{U_{SG,@LDA}}$ |
|---|---|---|---|---|

| | | | | |
|---|---|---|---|---|
| 5 | 5.0 | 1 | 6.22 | 1.24 |
| 5 | 5.0 | 3 | 6.24 | 1.24 |
| 5 | 5.0 | 5 | 6.23 | 1.24 |
| 5 | 5.0 | 7 | 6.20 | 1.23 |
| 6 | 6.0 | 1 | 7.52 | 1.25 |
| 7 | 7.1 | 1 | 8.86 | 1.25 |
| 7.5 | 7.6 | 1 | 9.25 | 1.22 |
| 8 | 8.1 | 1 | 10.1 | 1.25 |
| 10 | 10.2 | 1 | 12.5 | 1.23 |

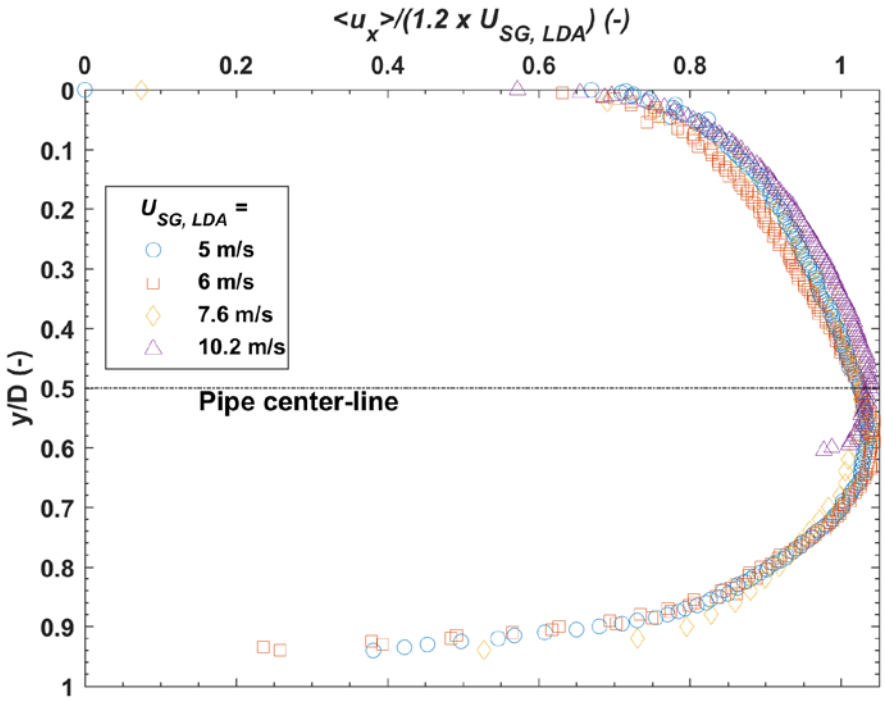


**Fig. 13.** Normalized droplet velocity profiles. Data is obtained using the LDA technique.

## 4. CONCLUSIONS

A careful experimental study has been performed to learn about the droplet flow field inside the gas space in low liquid loading flows. The measurements are conducted in a high-pressure flow loop using $SF_6$ as the gas phase and Exxsol D60 as the liquid phase. By utilizing the high-pressure flow loop, conditions approaching those

in a real gas-condensate pipeline are simulated. A non-intrusive LDA technique and intrusive isokinetic technique are used to measure the streamwise velocity field along the center-line. The main attention was given to conditions where the droplet entrainment (atomization) in the gas cross-sectional area varies from low to high. Several important conclusions can be reached from the current work:

- Under the studied conditions, single-phase gas flow characteristics are preserved close to the top pipe wall. The high spatial resolution of LDA allowed us to perform measurements close to the pipe wall.
- The time-averaged streamwise droplet velocity profiles show an asymmetric behavior, especially at the lowest $U_{SG}$ case (5 m/s). This asymmetric velocity profile may be due to the existence of thick liquid film, thereby decreasing the gas cross-sectional area. The other possibilities include turbulence modification and ballistic versus diffusive droplets. For the highest $U_{SG}$ case studied (10 m/s), a symmetric droplet velocity field is observed. Under this condition, there is a very thin liquid film (order of 0.5 mm or less), so the cross-sectional area of the gas is nearly equal to the pipe diameter.
- When the droplet flow field is asymmetric, the maximum droplet velocity is generally offset from the pipe center-line. These trends agree with stratified flow experimental data presented by Paras et al. (1997).
- The turbulent intensity profiles show a significant influence of the gas-liquid interfacial waves on the flow field. The very high turbulent intensity values are due to both high droplet concentration and interfacial waves.
- The dynamic pressure profiles obtained using the isokinetic probe also show the asymmetric behavior for the low gas velocity cases. There is a very good match between the droplet velocity measurements from the LDA and the isokinetic probe. The isokinetic probe can also be utilized to measure inside the high droplet concentration regions where the measurements from the LDA is challenging due to high light reflections.
- The normalized droplet velocity profiles indicate a near self-similar behavior regardless of the droplet entrainment condition in the gas space (low to high atomization conditions).

It is suggested to test the possible existence of secondary flows in low liquid loading flows. To confirm the existence of the secondary motion in the gas space, the velocity measurements in the wall normal direction along with axial direction should be made. Furthermore, we recommend performing flow field measurements inside the liquid film layer along with statistical characterization of the film thickness measurements. Additionally, it would be valuable to measure the gas velocity profiles in the presence of droplets, and compare the droplet velocity

profile to the gas velocity profile (to measure average slip velocity). This can be interesting especially in the lower half of the pipe, where the droplets do not follow the gas phase very well. The Stokes number will be well above unity, on average, considering all drop diameters. Finally, there should be more studies focused on cross-sectional liquid film thickness distribution and droplet size measurements. In addition to the knowledge obtained from the velocity measurements, the droplet size and film thickness information can be used to improve existing flow models.

# 5. NOMENCLATURE

| | |
|---|---|
| $C$ | Volume concentration [-] |
| $D$ | Pipe diameter [mm] |
| $f_E$ | Droplet entrained fraction [%] |
| $I_x$ | Streamwise turbulence intensity [%] |
| LDA | Laser Doppler Anemometer |
| $n$ | Number of measurement samples [-] |
| $P$ | Pressure [Pa] |
| $P_D$ | Dynamic pressure [Pa] |
| $q_D$ | Droplet volumetric flow rate [ml $s^{-1}$] |
| $R$ | Pipe radius [mm] |
| $Re$ | Reynolds number [-] |
| RMS | Root Mean Square |
| $T$ | System temperature [°C] |
| $u_\tau$ | Wall friction velocity [m $s^{-1}$] |
| $u^+$ | Dimensionless velocity [-] |
| $< u_x >$ | Streamwise mean droplet velocity [m $s^{-1}$] |
| $< u_x > \vert_{max}$ | Maximum droplet velocity [m $s^{-1}$] |
| $u_{D,i}$ | Instantaneous droplet velocity [m $s^{-1}$] |
| $U$ | Velocity [m $s^{-1}$] |
| $y$ | Distance from the Top Pipe Wall [mm] |
| $y^+$ | Dimensionless wall distance [-] |
| *Greek symbols* | |
| $\nabla P_{rel}$ | Increase in pressure drop, relative to single-phase [%] |
| $\eta$ | Refractive index [-] |
| $\theta$ | Pipe inclination [°] |
| $\kappa$ | von Kármán constant [-] |
| $\mu$ | Viscosity [mPa s] |
| $\rho$ | Density [kg $m^{-3}$] |
| $\tau$ | Shear stress [Pa] |
| *Subscripts* | |
| sys | System |
| G | Gas phase |
| L | Liquid phase |
| M | Mixture |
| W | Wall |
| SG | Superficial gas |
| SL | Superficial liquid |

# 6. REFERENCES


[1] Andreussi, P., Asali, J.C. and Hanratty, T.J., 1985. Initiation of roll waves in gas-liquid flows. AIChE J. 31(1), pp.119-126.

[2] Andritsos, N. and Hanratty, T.J., 1987. Influence of interfacial waves in stratified gas-liquid flows. AIChE J. 33(3), pp.444-454.

[3] Ayati, A.A., Kolaas, J., Jensen, A. and Johnson, G.W., 2014. A PIV investigation of stratified gas–liquid flow in a horizontal pipe. INT. J. Multiphase Flow 61, pp.129-143.

[4] Alamu, M.B. and Azzopardi, B.J., 2011. Simultaneous investigation of entrained liquid fraction, liquid film thickness and pressure drop in vertical annular flow. J. Energy Resour. Technol. 133(2), p.023103.

[5] Al-Sarkhi, A., Sarica, C. and Qureshi, B., 2012. Modeling of droplet entrainment in co-current annular two phase flow: A new approach. INT. J. Multiphase Flow 39, pp.21-28.

[6] Azzopardi, B.J., 1997. Drops in Annular Two phase Flow. INT. J. Multiphase Flow 23, 1–53.

[7] Bailey, S.C.C., Vallikivi, M., Hultmark, M. and Smits, A.J., 2014. Estimating the value of von Kármán's constant in turbulent pipe flow. J. Fluid. Mech. 749, pp.79-98.

[8] Gawas, K. 2013. Studies in low liquid loading in gas/oil/water three phase flow in horizontal and near-horizontal pipes. Doctoral dissertation, University of Tulsa, Tulsa, Oklahoma.

[9] Gawas, K., Karami, H., Pereyra, E., Al-Sarkhi, A. and Sarica, C., 2014. Wave characteristics in gas–oil two phase flow and large pipe diameter. INT. J. Multiphase Flow 63, pp.93-104.

[10] Hanratty, T.J. 2013. Physics of Gas-Liquid Flows. Cambridge University Press.

[11] Ishii, M. and Grolmes, M.A., 1975. Inception criteria for droplet entrainment in two-phase concurrent film flow. AIChE J. 21(2), pp.308-318.

[12] Ishii, M. and Mishima, K., 1989. Droplet entrainment correlation in annular two phase flow. Int. J. Heat Mass Transfer 32(10), pp.1835-1846.

[13] Karami, H., Pereyra, E., Torres, C.F. and Sarica, C., 2017. Droplet entrainment analysis of three phase low liquid loading flow. INT. J. Multiphase Flow 89, pp.45-56.

[14] Kesana, N.R., Skartlien, R., Langsholt, M., Ibarra, R., Tutkun. M., 2018. Droplet flux measurements in high pressure gas condensate low liquid loading horizontal pipe flow. (Under Review) Submitted to Journal of Natural Gas Science and Engineering.

[15] Magrini, K.L. 2009. Liquid Entrainment in Annular Gas/Liquid Flow in Inclined Pipes. MS thesis, University of Tulsa, Tulsa, Oklahoma.

[16] Magrini, K.L., Sarica, C., Al-Sarkhi, A. and Zhang, H.Q., 2012. Liquid entrainment in annular gas/liquid flow in inclined pipes. SPE Journal 17(02), pp.617-630.

[17] Mantilla, I. 2008. Mechanistic Modeling of Liquid Entrainment in Gas in Horizontal Pipes. Doctoral dissertation, University of Tulsa, Tulsa, Oklahoma.

[18] Pan, L. and Hanratty, T.J., 2002. Correlation of entrainment for annular flow in horizontal pipes. INT. J. Multiphase Flow 28(3), pp.385-408.

[19] Paras, S.V., Vlachos, N.A. and Karabelas, A.J., 1998. LDA measurements of local velocities inside the gas phase in horizontal stratified/atomization two-phase flow. INT. J. Multiphase Flow 24(4), pp.651-661.

[20] Vuong, D.H., Sarica, C., Pereyra, E. and Al-Sarkhi, A., 2018. Liquid droplet entrainment in two-phase oil-gas low-liquid-loading flow in horizontal pipes at high pressure. INT. J. Multiphase Flow 99, pp.383-396.

[21] Sawant, P., Ishii, M. and Mori, M., 2008. Droplet entrainment correlation in vertical upward co-current annular two phase flow. Nucl. Eng. Des. 238(6), pp.1342-1352.

[22] Setyawan, A., Indarto, Deendarlianto, 2016. The effect of the fluid properties on the wave velocity and wave frequency of gas–liquid annular two-phase flow in a horizontal pipe. Exp. Therm Fluid Sci. 71, pp.25-41.

[23] Skartlien, R., Nuland, S. and Amundsen, J.E., 2011. Simultaneous entrainment of oil and water droplets in high Reynolds number gas turbulence in horizontal pipe flow. INT. J. Multiphase Flow 37(10), pp.1282-1293.

[24] Schubring, D., Ashwood, A.C., Shedd, T.A. and Hurlburt, E.T., 2010. Planar laser-induced fluorescence (PLIF) measurements of liquid film thickness in annular flow. Part I: Methods and data. INT. J. Multiphase Flow 36(10), pp.815-824.

[25] Sheikholeslami, M. and Ganji, D.D., 2016. Heat transfer enhancement in an air to water heat exchanger with discontinuous helical turbulators; experimental and numerical studies. Energy 116, pp.341-352.

[26] Tayebi, D., Nuland, S. and Fuchs, P., 2000. Droplet transport in oil/gas and water/gas flow at high gas densities. INT. J. Multiphase Flow 26(5), pp.741-761.

[27] Tzotzi, C. and Andritsos, N., 2013. Interfacial shear stress in wavy stratified gas–liquid flow in horizontal pipes. INT. J. Multiphase Flow, 54, pp.43-54.

## Acknowledgements

This work is performed as a part of an ongoing project titled “Condition monitoring tool for separators based on combined use of tracer technology and Multiphase flow modeling”. The support from The Research Council of Norway, and from the industrial partners: Statoil AS and Aker BP are gratefully acknowledged. The authors would like to thank Dr. Jan Nossen at IFE for his constructive comments to improve the manuscript.